

## RADIO ASTRONOMICAL POLARIMETRY AND POINT-SOURCE CALIBRATION

W. VAN STRATEN  
Netherlands Foundation for Research in Astronomy  
straten@astron.nl  
*Draft version November 8, 2018*

### ABSTRACT

A mathematical framework is presented for use in the experimental determination of the polarimetric response of observatory instrumentation. Elementary principles of linear algebra are applied to model the full matrix description of the polarization measurement equation by least-squares estimation of non-linear, scalar parameters. The formalism is applied to calibrate the center element of the Parkes Multibeam receiver using observations of the millisecond pulsar, PSR J0437–4715, and the radio galaxy, 3C 218 (Hydra A).

*Subject headings:* methods: data analysis — instrumentation: polarimeters — polarization — pulsars: individual (PSR J0437-4715) — techniques: polarimetric

### 1. INTRODUCTION

Polarization measurements provide additional insight into the phenomena involved in both the emission and propagation of electromagnetic radiation. However, the processes of reception and detection introduce instrumental artifacts that must be corrected before meaningful interpretations of experimental data can be made. Ideally, the instrumental response is estimated by observing at least two calibrator sources of well-determined, polarized radiation (Hamaker, Bregman & Sault 1996). Under the assumption that the observatory apparatus respond linearly and remain stable between calibrator observations, the known instrumental response is then inverted and used to calibrate observations of other sources.

In the absence of a sufficient number of calibrator sources, instrumental calibration may in some cases be performed by fitting the available polarimetric data to a predictive model. This model must describe the observed sources of radiation, the response of the instrument, and any additional propagation effects that arise in the intervening media through which the signals are transmitted, such as the Earth's ionosphere. In order for the model to be constrained, at least one component of the applied measurement equation must vary as some function of one or more independent variables. For example, the constraining transformation may consist of the geometric projection of the antenna receptors onto the plane of the sky, which may vary during transit of the source for antennas without an equatorial mount.

For an altitude-azimuth mounted antenna, the receiver feed is rotated about the line of sight through the parallactic angle, a constraint that has been utilized in a number of previous studies, including Stinebring et al. (1984), Turlo et al. (1985), Xilouris (1991), McKinnon (1992), and Johnston (2002). In each of these cases, a matrix product is expanded to yield a set of scalar equations that describe the measured Stokes parameters as a function of parallactic angle; these are then solved using conventional techniques. This approach has two significant limitations. First, in order to simplify the derivation of the scalar equations and their partial derivatives, it is necessary to make small value approximations that are not generally valid.

Second, as any alteration of the reception model necessitates a laborious expansion of the matrix product, this approach is non-conducive to experimentation with a variety of parameterizations.

In addition to these shortcomings, other fundamental limitations and conceptual errors have been incorporated into previous treatments. For instance, Turlo et al. (1985) omit circular polarization from consideration, an oversimplification that restricts further application of their result to antenna with perfect, circularly polarized receptors. Stinebring et al. (1984), followed by Xilouris (1991) and McKinnon (1992), begin with the assumption that the complex gains of the two polarizations may be independently calibrated prior to determination of the cross-coupled antenna response. However, this approximation is accurate only when the differential gain and phase transformations commute with the antenna response matrix, a condition satisfied only when the feed receptors have well-determined, orthogonal polarizations. In general, the complex gains may be accurately quantified only after the effect of the antenna feed is included.

This error is essentially compounded in Johnston (2002) where, although the instrumental response parameters are jointly estimated, the measured data are first corrected using separately-determined, inaccurate estimates of differential gain and phase. In addition, the observed Stokes parameters are incorrectly normalized by the total intensity; a quantity such as the invariant interval must be used (Stinebring et al. 1984; Britton 2000). Finally, as only observations of an unknown source are used to constrain the instrumental response parameters, the solution derived by Johnston (2002) is not unique. Rather, as shown in Appendix B, there exists a degenerate set of solutions that can be resolved only with additional observations of one or more sources with known circular polarization and position angle.

In contrast to previous work, the treatment presented in this paper is based entirely on a full matrix description of the polarization measurement equation. All of the matrix products, including those of the required partial derivatives, are evaluated in software; therefore, no small value approximations are necessary and a variety of model spec-

ifications may be tested with relative ease. Furthermore, all of the model parameters are jointly constrained using observations of both unknown and partially known source polarizations. Following a brief mathematical review in Section 2, the method employed to solve the matrix equations is developed in Section 3. Two possible decompositions of the instrumental response are described in Section 4, one of which is applied in Section 5 to the calibration of the Multibeam receiver and downconversion system utilized by CPSR-II: the 128 MHz baseband recording and real-time processing system at the Parkes Observatory.

## 2. POLARIZED RADIATION AND PROPAGATION

Electromagnetic radiation is described by the two complex-valued components of the transverse electric field vector,  $\mathbf{e}(t) = (e_0(t), e_1(t))$ . The measurable properties of  $\mathbf{e}(t)$  are represented by the coherency matrix,  $\boldsymbol{\rho} = \langle \mathbf{e}(t) \otimes \mathbf{e}^\dagger(t) \rangle$ , where the angular brackets denote time averaging and  $\mathbf{e}^\dagger$  is the Hermitian transpose of  $\mathbf{e}$ . The coherency matrix may be written as a linear combination of Hermitian basis matrices (Britton 2000),

$$\boldsymbol{\rho} = \frac{1}{2} \sum_{k=0}^3 S_k \boldsymbol{\sigma}_k = (S_0 \boldsymbol{\sigma}_0 + \mathbf{S} \cdot \boldsymbol{\sigma})/2, \quad (1)$$

where  $\boldsymbol{\sigma}_0$  is the  $2 \times 2$  identity matrix,  $\boldsymbol{\sigma} = (\boldsymbol{\sigma}_1, \boldsymbol{\sigma}_2, \boldsymbol{\sigma}_3)$  are the Pauli spin matrices,  $S_0$  is the total intensity, or Stokes  $I$ , and  $\mathbf{S} = (S_1, S_2, S_3)$  is the Stokes polarization vector. As described in Appendix A,  $\mathbf{S} = (Q, U, V)$  in the Cartesian reference frame applied in this paper. The Stokes parameters may also be expressed in terms of the coherency matrix (Hamaker 2000),

$$S_k = \text{tr}(\boldsymbol{\sigma}_k \boldsymbol{\rho}), \quad (2)$$

where  $\text{tr}(\mathbf{A})$  is the trace of the matrix,  $\mathbf{A}$ .

The propagation and reception of the electric field is represented by the transformations of linear time-invariant systems. Presented with the input signal,  $\mathbf{e}(t)$ , the output of a system is given by the convolution,  $\mathbf{e}'(t) = \mathbf{j}(t) * \mathbf{e}(t)$ , where  $\mathbf{j}(t)$ , is the complex-valued,  $2 \times 2$  impulse response matrix. By the convolution theorem, this transformation is equivalent to  $\mathbf{E}'(\omega) = \mathbf{J}(\omega) \mathbf{E}(\omega)$ , where  $\mathbf{J}$  is the familiar Jones matrix. When observed over a sufficiently narrow band, the variation of  $\mathbf{J}$  with frequency is ignored, and polarimetric transformations are represented by Jones matrix multiplications in the time domain. Under the operation,  $\mathbf{e}'(t) = \mathbf{J} \mathbf{e}(t)$ , the coherency matrix is transformed as

$$\boldsymbol{\rho}' = \mathbf{J} \boldsymbol{\rho} \mathbf{J}^\dagger. \quad (3)$$

This congruence transformation is called the polarization measurement equation (Hamaker 2000). It forms the basis through which measured quantities are related to the intrinsic polarizations of the sources and used to model the unknown instrumental response.

## 3. MAXIMUM LIKELIHOOD ESTIMATOR

To solve the polarization measurement equation using conventional methods of least-squares minimization, it is necessary to design a scalar figure-of-merit function and to calculate both its gradient and curvature with respect to scalar model parameters. Let  $\boldsymbol{\eta}$  represent the vector of scalar parameters that describe the model, including the

instrumental response and the polarizations of the sources. Furthermore, let  $\mathbf{x}$  represent the vector of independent variables that constrain the measurement equation, such as the observing frequency and epoch. Given  $\mathbf{x}$ , the model,

$$\boldsymbol{\rho}'_m(\mathbf{x}; \boldsymbol{\eta}); \quad 1 \leq m \leq M, \quad (4)$$

must predict the measured polarization of each source, where  $M$  is the number of sources. In the interest of brevity, the model may also be represented by  $\boldsymbol{\rho}'_m(\mathbf{x})$ .

Now consider  $N_m$  independent observations of the  $m^{\text{th}}$  source, each made at a unique coordinate,  $\mathbf{x}_{m,n}$ , to yield the measured Stokes parameters and their estimated errors,  $\{S'_k \pm \sigma_k\}_{m,n}$ . The best-fit model parameters will minimize the objective merit function,

$$\chi^2(\boldsymbol{\eta}) = \sum_{m=1}^M \sum_{n=1}^{N_m} \sum_{k=0}^3 \frac{[S'_{k,m,n} - S'_{k,m}(\mathbf{x}_{m,n}; \boldsymbol{\eta})]^2}{\sigma_{k,m,n}^2}, \quad (5)$$

where  $S'_{k,m}(\mathbf{x}_{m,n}; \boldsymbol{\eta}) = \text{tr}[\boldsymbol{\sigma}_k \boldsymbol{\rho}'_m(\mathbf{x}_{m,n}; \boldsymbol{\eta})]$  are the Stokes parameters of the  $m^{\text{th}}$  source as predicted by the model at  $\mathbf{x}_{m,n}$ . The gradient of  $\chi^2$  with respect to the scalar parameters,  $\boldsymbol{\eta}$ , has components,

$$\frac{\partial \chi^2}{\partial \eta_r} = -2 \sum_{m=1}^M \sum_{n=1}^{N_m} \text{tr} \left( \boldsymbol{\Delta}_{m,n}(\boldsymbol{\eta}) \frac{\partial \boldsymbol{\rho}'_m(\mathbf{x}_{m,n}; \boldsymbol{\eta})}{\partial \eta_r} \right), \quad (6)$$

where

$$\boldsymbol{\Delta}_{m,n}(\boldsymbol{\eta}) = \sum_{k=0}^3 \frac{S'_{k,m,n} - S'_{k,m}(\mathbf{x}_{m,n}; \boldsymbol{\eta})}{\sigma_{k,m,n}^2} \boldsymbol{\sigma}_k. \quad (7)$$

Taking an additional partial derivative yields

$$\frac{\partial^2 \chi^2}{\partial \eta_s \partial \eta_r} = -2 \sum_{m=1}^M \sum_{n=1}^{N_m} \text{tr} \left( \frac{\partial \boldsymbol{\Delta}_{m,n}}{\partial \eta_s} \frac{\partial \boldsymbol{\rho}'_m(\mathbf{x}_{m,n})}{\partial \eta_r} \right), \quad (8)$$

where, following the discussion in §15.5 of Numerical Recipes (Press et al. 1992), the term containing a second derivative in equation (8) has been eliminated. Using equations (5) through (8), the Levenberg-Marquardt method is applied to find the parameters that minimize  $\chi^2(\boldsymbol{\eta})$ .

## 4. PARAMETERIZATION OF THE MODEL

It remains to specify the scalar values,  $\boldsymbol{\eta}$ , that parameterize the polarization measurement equation as well as the partial derivatives of  $\boldsymbol{\rho}'_m(\mathbf{x}; \boldsymbol{\eta})$  with respect to those parameters. As in equation (1), the coherency matrix,  $\boldsymbol{\rho}_m$ , of each input source polarization is completely specified by the four Stokes parameters,  $S_{k,m}$ . The partial derivatives with respect to these parameters are simply

$$\frac{\partial \boldsymbol{\rho}_m}{\partial S_{k,m}} = \frac{\boldsymbol{\sigma}_k}{2}. \quad (9)$$

Now, let the model of the instrumental response be represented by the complex-valued  $2 \times 2$  Jones matrix,  $\mathbf{J}$ . If  $\mathbf{J}$  satisfies equation (3) then it belongs to the set of solutions given by  $\mathbf{J}(\phi) = e^{i\phi} \mathbf{J}$ , where  $i = \sqrt{-1}$ . That is, the coherency matrix is insensitive to the absolute phase of the signal and  $\phi$  may be arbitrarily chosen, leaving seven degrees of freedom with which to describe the instrumental response. Two possible parameterizations are considered: the algebraic decomposition employed by Hamaker (2000) and the phenomenological description of Britton (2000).

## 4.1. Algebraic Model

Following Hamaker (2000), an arbitrary matrix,  $\mathbf{J}$ , is represented by its polar decomposition,

$$\mathbf{J} = J \mathbf{B}_{\hat{\mathbf{m}}}(\beta) \mathbf{R}_{\hat{\mathbf{n}}}(\phi) \quad (10)$$

where  $J = (\det \mathbf{J})^{1/2}$  and, as described in Appendix A,

$$\mathbf{B}_{\hat{\mathbf{m}}}(\beta) = \cosh \beta \boldsymbol{\sigma}_0 + \sinh \beta \hat{\mathbf{m}} \cdot \boldsymbol{\sigma}, \quad (11)$$

$$\mathbf{R}_{\hat{\mathbf{n}}}(\phi) = \cos \phi \boldsymbol{\sigma}_0 + i \sin \phi \hat{\mathbf{n}} \cdot \boldsymbol{\sigma}. \quad (12)$$

The phase of the complex value,  $J$ , is set to zero and, as any rotation about an arbitrary axis may be decomposed into a series of rotations about three perpendicular axes, the instrumental response is written as

$$\mathbf{J}_H = G \mathbf{B}_{\hat{\mathbf{m}}}(\beta) \prod_{k=1}^3 \mathbf{R}_{\hat{\mathbf{s}}_k}(\phi_k), \quad (13)$$

where  $G = |J|$  is the absolute gain and  $\hat{\mathbf{s}}_k$  are the orthonormal basis vectors defined in Appendix A. Equation (11) may be written as  $\mathbf{B}_{\hat{\mathbf{m}}}(\beta) = b_0 \boldsymbol{\sigma}_0 + \mathbf{b} \cdot \boldsymbol{\sigma}$ , where  $b_0 = \cosh \beta$  and  $\mathbf{b} = \sinh \beta \hat{\mathbf{m}}$ . Noting that  $b_0 \geq 1$  and  $b_0^2 = 1 + \mathbf{b} \cdot \mathbf{b}$ , the three degrees of freedom of  $\mathbf{B}_{\hat{\mathbf{m}}}(\beta)$  are specified by  $\mathbf{b} = (b_1, b_2, b_3)$ . Therefore, the instrumental response is parameterized by  $G$ ,  $b_{1-3}$ , and  $\phi_{1-3}$ . The partial derivatives of  $\mathbf{J}_H$  with respect to these seven parameters are calculated using products of

$$\frac{\partial \mathbf{B}_{\hat{\mathbf{m}}}(\beta)}{\partial b_k} = \frac{b_k}{\sqrt{1 + \mathbf{b} \cdot \mathbf{b}}} \boldsymbol{\sigma}_0 + \boldsymbol{\sigma}_k, \quad (14)$$

and

$$\frac{\partial \mathbf{R}_{\hat{\mathbf{s}}_k}(\phi_k)}{\partial \phi_k} = -\sin \phi_k \boldsymbol{\sigma}_0 + i \cos \phi_k \boldsymbol{\sigma}_k. \quad (15)$$

## 4.2. Phenomenological Model

Beginning with Britton (2000), the response of an ideal feed with two orthogonally polarized receptors is given by  $\mathbf{S}(\theta, \epsilon) = \mathbf{R}_{\hat{\mathbf{a}}}(\epsilon) \mathbf{R}_{\hat{\mathbf{b}}}(\theta)$ . Here, the receptors have ellipticities equal to  $\epsilon$  and mutually perpendicular orientations defined by  $\theta$ . The basis vectors,  $\hat{\mathbf{q}}$ ,  $\hat{\mathbf{u}}$ , and  $\hat{\mathbf{v}}$ , are defined in Appendix A. Using this notation, a receiver with non-orthogonal receptors is represented by

$$\mathbf{C} = \boldsymbol{\delta}_0 \mathbf{S}(\theta_0, \epsilon_0) + \boldsymbol{\delta}_1 \mathbf{S}(\theta_1, \epsilon_1), \quad (16)$$

where  $\boldsymbol{\delta}_a$  is the  $2 \times 2$  selection matrix,

$$\boldsymbol{\delta}_a = \begin{pmatrix} \delta_{0a} & 0 \\ 0 & \delta_{1a} \end{pmatrix}, \quad (17)$$

$\delta_{ab}$  is the Kronecker delta, and the product,  $\boldsymbol{\delta}_a \mathbf{B}$ , returns a matrix that contains only the  $a^{\text{th}}$  row of  $\mathbf{B}$ . Equation (16) is equivalent to equation 16 of Britton (2000) and is used without making any first order approximations or further assumptions about the feed.

The differential gain and phase of the instrument are represented by  $\mathbf{B}_{\hat{\mathbf{s}}_1}(\gamma)$  and  $\mathbf{R}_{\hat{\mathbf{s}}_1}(\varphi)$  where, as in equations (A1) and (A2),  $\gamma$  and  $\varphi$  parameterize Lorentz boost and rotation transformations (Britton 2000). Including the absolute gain,  $G$ , the instrumental response is written as

$$\mathbf{J}_B = G \mathbf{B}_{\hat{\mathbf{s}}_1}(\gamma) \mathbf{R}_{\hat{\mathbf{s}}_1}(\varphi) \mathbf{C}. \quad (18)$$

The partial derivatives of  $\mathbf{J}_B$  with respect to its seven scalar parameters,  $G$ ,  $\gamma$ ,  $\varphi$ ,  $\theta_{0-1}$ , and  $\epsilon_{0-1}$ , are calculated using equation (15) and

$$\frac{\partial \mathbf{B}_{\hat{\mathbf{s}}_k}(\beta_k)}{\partial \beta_k} = \sinh \beta_k \boldsymbol{\sigma}_0 + \cosh \beta_k \boldsymbol{\sigma}_k. \quad (19)$$

## 5. APPLICATION

Radio pulsar observations provide an excellent source of data with which to constrain the polarization measurement equation. The often highly polarized state of a pulsar signal can vary significantly as a function of pulse longitude. When integrated over a sufficient number of spin periods, mean polarimetric pulse profiles generally exhibit excellent stability on timescales much longer than those over which calibration observations are made. Consequently, multiple on-pulse longitudes from a single pulsar may be included as unique and stable input source polarizations, greatly increasing the number of available constraints when compared with non-pulsed sources. Furthermore, any non-pulsed background polarization is effectively eliminated by subtracting the off-pulse mean from each integrated pulse profile.

The millisecond pulsar, PSR J0437–4715, represents an ideal candidate for use in the regular calibration of the apparatus at the Parkes Observatory. As part of the high-precision pulsar timing program, it is often observed from rise to set, providing measurements with a wide range in parallactic angle. The model that describes these observations has the form,

$$\boldsymbol{\rho}'_m(\Phi) = \mathbf{J} \mathbf{R}_{\hat{\mathbf{e}}}(\Phi) \boldsymbol{\rho}_m \mathbf{R}_{\hat{\mathbf{e}}}^\dagger(\Phi) \mathbf{J}^\dagger, \quad (20)$$

where  $\mathbf{R}_{\hat{\mathbf{e}}}(\Phi)$  is the rotation about the line of sight by the parallactic angle,  $\Phi$ .

As demonstrated in Appendix B, additional calibrator observations are required in order to uniquely determine the solution to equation (20). The Parkes Multibeam receiver is equipped with a noise diode that ideally injects a 100% linearly polarized signal with a position angle of 45 degrees into the receiver feed horn. This reference source is switched using a signal generator and the observed square waveform is integrated modulo its period. Ideally, the on-pulse longitudes of the input reference signal contain additional flux with Stokes parameters given by  $C_0[1, 0, 1, 0]$ , where  $C_0$  is the reference flux density. Under this assumption, inclusion of reference signal observations breaks the degeneracy by constraining the boost,  $\beta_v$ , which mixes Stokes  $I$  and  $V$ , and the rotation,  $\phi_v$ , which mixes Stokes  $Q$  and  $U$ . In a separate flux calibration procedure, the reference signal is observed simultaneously with the bright Fanaroff-Riley type I radio galaxy, 3C 218 (Hydra A), producing absolute flux estimates of both the system temperature and reference flux density,  $C_0$ .

## 5.1. Observations

Dual-polarization observations of PSR J0437–4715 and Hydra A were made on 19 and 20 July 2003 using the center element of the Parkes Multibeam receiver. Two 64 MHz bands, centered at 1341 and 1405 MHz, were two-bit sampled and processed by CPSR-II, the second generation of the Caltech-Parkes-Swinburne Recorder. In order to maintain optimal linear response during the digitization process, the detected power is monitored and the sampling thresholds are updated approximately every 30 seconds. In addition, the baseband data reduction software corrects quantization distortions to the voltage waveform using the dynamic level-setting technique (Jenet & Anderson 1998).

Phase-coherent dispersion removal is performed while synthesizing a 128-channel filterbank (Jenet et al. 1997); the Stokes parameters are then detected and integrated as a function of topocentric pulse phase. Data are averaged for five minute intervals, producing uncalibrated mean pulse profiles with 2048 phase bins, or an equivalent time resolution of approximately  $2.8 \mu\text{s}$ .

The observed flux density varies significantly between pulsar and Hydra A observations, resulting in large changes to the digitization sampling thresholds. This difference is best modeled using the phenomenological decomposition of equation (18), applying separate absolute gain, differential gain, and differential phase terms to the two sets of observations. Also, in order to account for phase drifts on timescales of a few hours, the differential phase is modeled to vary as a cubic polynomial function of time. The three signal path transformations corresponding to the three observed sources are summarized in Table 1.

The flux of the pulsar also varies between observations, a result of both intrinsic intensity fluctuations and interstellar scintillation. Therefore, the measured Stokes parameters are normalized by the invariant interval,

$$S'_{\text{inv}} = 2(\det \rho'_{m,n})^{1/2} = (S_0'^2 - S'^2)^{1/2}, \quad (21)$$

where the polarized intensity,  $S' = |\mathbf{S}'|$ . In order to avoid division by small or negative values, those data points with  $S'_{\text{inv}} < \sigma_0$  are discarded. Assuming that the measurement errors in each of the Stokes parameters are independent of each other, the estimated errors in the normalized Stokes parameters are given by

$$\hat{\sigma}_0^2 = S_{\text{inv}}'^{-6} S'^2 (S'^2 \sigma_0^2 + S_0'^2 \sigma_s^2), \quad \text{and} \quad (22)$$

$$\hat{\sigma}_k^2 = S_{\text{inv}}'^{-4} [(S_{\text{inv}}'^2 + 2S_k'^2) \sigma_k^2 + S_k'^2 \sigma_{\text{inv}}^2], \quad (23)$$

where  $1 \leq k \leq 3$ ,

$$S'^2 \sigma_s^2 = \sum_{k=1}^3 S_k'^2 \sigma_k^2, \quad (24)$$

and  $S_{\text{inv}}'^2 \sigma_{\text{inv}}^2 = S_0'^2 \sigma_0^2 + S'^2 \sigma_s^2$ . Note that  $\hat{\sigma}_0$  is approximately proportional to  $S'$  when  $S' \ll S_0$ . Consequently, the normalized total intensity is plotted on a separate scale in Figure 1, in which are displayed the normalized Stokes parameters from one of the 65 pulse longitudes used to constrain the model.

## 5.2. Results

Initial results indicated that the reference signal produced by the noise diode of the Parkes Multibeam receiver is not actually 100% linearly polarized. Rather, as shown in Figure 2, the reference signal consists of  $\sim 90\%$  linear and  $3\%$  circular polarization, its position angle is not exactly 45 degrees (i.e. Stokes  $Q \neq 0$ ), and it is severely depolarized at the edges of the band due to frequency aliasing during downconversion. Consequently, the reference signal cannot be trusted as a source with known position angle and degree of circular polarization. Also, approximately 7 MHz from both the top and bottom of the band must be discarded as irreversibly corrupted.

In order to constrain  $\beta_v$ , it is noted that Hydra A has less than 0.1% circular polarization (Roberts et al. 1975). Therefore, the off-pulse longitudes of the flux calibration observations serve as a source of negligible circular polarization in the remainder of this development. The unknown rotation about the line of sight,  $\phi_v$ , is artificially

constrained by assuming that  $\theta_0 = 0$ ; consequently, all position angles are measured with respect to the orientation of receptor 0. In modeling the reference signal, Stokes  $I$  is set to unity, producing an intermediate flux scale in units of the reference flux density; Stokes  $Q$ ,  $U$ , and  $V$  are varied as free model parameters.

The reception model is solved independently for each of the 256 frequency channels in the two 64 MHz bands. In each channel are a total of 278 free model parameters, corresponding to the Stokes parameters of the 65 selected pulse longitudes, the 12 instrumental parameters listed in Table 1, and the 6 unknown Stokes parameters shared between the noise diode and Hydra A. These parameters are constrained by approximately 25220 measured values, primarily derived from the selected pulse longitudes of the 97 pulsar observations. Indicating a good fit in each frequency channel, the merit function is on average approximately equal to the number of degrees of freedom,  $\nu$ , such that  $\langle \chi^2/\nu \rangle \sim 1.05$ . Under the assumption that the errors in the measured Stokes parameters are normally distributed, the curvature matrix of equation (8) is inverted to yield the covariance matrix of the standard errors in each of the model parameters.

In Figure 3 are plotted the instrumental response parameters from one of the CPSR-II bands at the reference epoch. The linear dependence between differential phase and frequency indicates a signal path length mismatch between the two polarizations. The receptor ellipticities have an average value of  $\sim 5.7$  degrees, corresponding to a rotation of the polarization vector about the  $U$ -axis by  $\sim 0.2$  radians. Consequently, the degree of mixing between linear and circular polarizations reaches approximately 20% for uncalibrated signals with polarization vectors lying near the  $Q - V$  plane. Clearly, this level of distortion cannot be treated as a second-order effect.

The mean polarimetric pulse profile of PSR J0437–4715 is plotted in Figure 4. Here, the position angle is equal to  $\theta$  and the colatitude is given by  $\pi/2 - 2\epsilon$ . When compared with cylindrical coordinates, as plotted in Figure 3 of van Straten (2002), spherical coordinates offer a number of conceptual advantages. For instance, both the total and polarized intensities may be plotted on the same logarithmic scale, thereby enhancing the smaller features of these profiles. In addition, the chosen normalization allows the statistical significance of the measured quantities to be approximated without explicitly plotting the estimated error bars. Finally, the correlations between rapid transitions in position angle and dips in polarized intensity are more obviously apparent, for example, at pulse phases approximately equal to 0.26, 0.50, and 0.84. These regions are interpreted as transitions between two highly polarized, nearly orthogonal, superposed modes of radiation, possibly the natural modes of the pulsar magnetospheric plasma (Petrova 2001, and references therein).

## 6. CONCLUSIONS

A fundamentally different approach to modeling the reception and propagation of polarized radiation has been presented in this paper. Based on the formalism developed in Sections 3 and 4, a detailed calibration model has

been constructed from simple, modular components, incorporating multiple signal paths and source polarizations as constraints. Many of the limiting assumptions made in previous treatments have been eliminated in this analysis, enabling its application in a wider variety of experiments. This development is increasingly relevant in the context of design considerations for the next generation of radio telescopes and instrumentation. For instance, it has been proposed that the Square Kilometer Array (SKA) will be an interferometric array of a large number of low-cost antennas. Especially in the case of fixed dipole pairs, the polarizations of the receptors may be highly non-orthogonal; therefore, it is important to develop more sophisticated theories and techniques of polarimetric calibration.

Due to the current lack of a standard catalog of multi-frequency polarimetric pulse profiles, it is difficult to confirm the validity of any calibration technique. Future efforts should include the establishment of a set of well-calibrated sources, including a number of stable pulsars that are monitored on a regular basis at more than one observatory and at a variety of radio frequencies. Especially at lower frequencies, other propagation effects such as those arising in the ionosphere will have to be included in the reception model applied to these observations. Once established, a relatively short integration on a bright, calibrated pulsar could be used to quickly determine the instrumental response without the need for time-intensive techniques such as the one described in this paper.

In order that the results presented in Section 5.2 may be used to calibrate other observations, they are stored as binary table extensions of a PSRFITS file (Hotan, van Straten & Manchester 2004), a pulsar data format defined using the Flexible Image Transport System (Hanisch et al. 2001). Both the PSRFITS file format and its associated visualization and reduction software have been openly developed in an effort to facilitate the exchange of pulsar astro-

nomical data between observatories and research groups.

As the current work is based on the Jones calculus, it is limited to describing only “non-depolarizing” or “pure” component transformations; it is not possible to represent the conversion of a fully polarized signal into a partially polarized one using Jones operators (Hamaker, Bregman & Sault 1996). This is demonstrated by noting that  $\det(\mathbf{AB}) = \det(\mathbf{A})\det(\mathbf{B})$  and, for a fully polarized signal,  $\det(\boldsymbol{\rho}) = 0$ . Certain components of the instrumental apparatus may not be pure and therefore may require a Mueller matrix in order to model their effect. For example, the process of two-bit quantization may act to depolarize strong input signals, an effect that has yet to be studied in rigorous detail. Other phenomena, such as bandwidth depolarization, may not require a Mueller matrix description if they can be treated by the application of phase-coherent matrix convolution (van Straten 2002).

The formalism developed in this paper may be equally well applied to the polarimetric calibration of a phased array. In this case, it is not necessary to describe the complete instrument in terms of the complex gains, orientations, and ellipticities of its individual receptors. Rather, it is more useful to consider only the total instrumental transformation given by the sum of the Jones matrices of the individual antennas. This development will be the subject of future work.

The Parkes Observatory is part of the Australia Telescope which is funded by the Commonwealth of Australia for operation as a National Facility managed by CSIRO. This research greatly benefited from lectures presented by Johan Hamaker from 14 January to 18 March, 2003. Thanks also to the Swinburne University of Technology Pulsar Group for providing the CPSR-II observations and to Ben Stappers for advice on the text.

## APPENDIX

### GEOMETRIC INTERPRETATION

The  $2 \times 2$  complex matrices with unit determinant may be parameterized by  $\exp[(\beta \hat{\mathbf{m}} + i\phi \hat{\mathbf{n}}) \cdot \boldsymbol{\sigma}]$ . The unit vectors,  $\hat{\mathbf{m}}$  and  $\hat{\mathbf{n}}$ , as well as the dimensionless values,  $\beta$  and  $\phi$ , have meaningful geometric interpretations in the four-dimensional space of the Stokes parameters. Under the congruence transformation of equation (3), the Hermitian matrices,

$$\mathbf{B}_{\hat{\mathbf{m}}}(\beta) = \exp(\beta \hat{\mathbf{m}} \cdot \boldsymbol{\sigma}) = \cosh \beta \sigma_0 + \sinh \beta \hat{\mathbf{m}} \cdot \boldsymbol{\sigma}, \quad (\text{A1})$$

effect a Lorentz boost of the Stokes 4-vector along the axis  $\hat{\mathbf{m}}$  by an impact parameter  $2\beta$ . Likewise, the unitary matrices,

$$\mathbf{R}_{\hat{\mathbf{n}}}(\phi) = \exp(i\phi \hat{\mathbf{n}} \cdot \boldsymbol{\sigma}) = \cos \phi \sigma_0 + i \sin \phi \hat{\mathbf{n}} \cdot \boldsymbol{\sigma}, \quad (\text{A2})$$

rotate the Stokes polarization vector about the axis  $\hat{\mathbf{n}}$  by an angle  $2\phi$ . In applying this geometric representation, the following conventions are used. First, the Pauli spin matrices are defined as

$$\boldsymbol{\sigma}_1 = \begin{pmatrix} 1 & 0 \\ 0 & -1 \end{pmatrix} \boldsymbol{\sigma}_2 = \begin{pmatrix} 0 & 1 \\ 1 & 0 \end{pmatrix} \boldsymbol{\sigma}_3 = \begin{pmatrix} 0 & -i \\ i & 0 \end{pmatrix}. \quad (\text{A3})$$

Second, the three-dimensional space of the Stokes polarization vector,  $\mathbf{S} = (S_1, S_2, S_3)$ , is spanned by the orthonormal basis vectors,  $\hat{\mathbf{s}}_k$ , such that  $\hat{\mathbf{s}}_k \cdot \mathbf{S} = S_k$  and  $\hat{\mathbf{s}}_k \cdot \boldsymbol{\sigma} = \boldsymbol{\sigma}_k$ . Finally, Stokes  $Q$ ,  $U$ , and  $V$  are calculated by the projection of  $\mathbf{S}$  onto the Stokes unit vectors,  $\hat{\mathbf{q}}$ ,  $\hat{\mathbf{u}}$ , and  $\hat{\mathbf{v}}$ , respectively. This relationship is summarized by  $\mathbf{p} = (Q, U, V) = \mathbf{R}^T \mathbf{S}$ , where  $\mathbf{R} = (\hat{\mathbf{q}} \hat{\mathbf{u}} \hat{\mathbf{v}})$  is a three-dimensional rotation matrix with columns defined by the Stokes unit vectors. The orientation of these basis vectors with respect to  $\hat{\mathbf{s}}_k$  depends upon the reference frame in which the electric field vector is represented. In the Cartesian basis, the plane wave propagates along the  $z$ -axis, the electric field is decomposed into its projection along the  $x$  and  $y$  axes, and  $\mathbf{R}$  is equal to the  $3 \times 3$  identity matrix.

TABLE 1  
SIGNAL PATH TRANSFORMATIONS

Source	Transformation
Noise Diode	$\mathbf{J}(t) = G \mathbf{B}_{\hat{s}_1}(\gamma) \mathbf{R}_{\hat{s}_1}(\varphi(t)) \mathbf{C}$
PSR J0437–4715	$\mathbf{J}(t) \mathbf{R}_{\hat{\phi}}(\Phi)$
3C 218	$G_H \mathbf{B}_{\hat{s}_1}(\gamma_H) \mathbf{R}_{\hat{s}_1}(\varphi_H) \mathbf{C}$

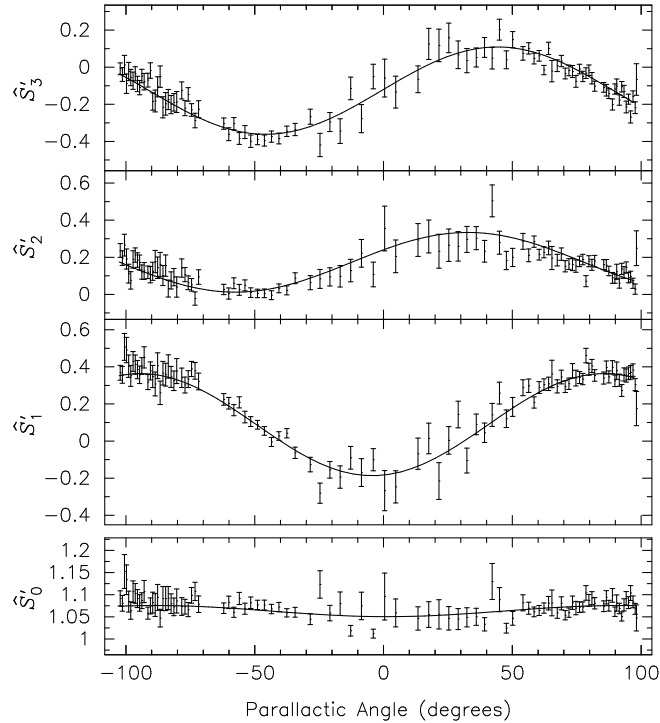


FIG. 1.— Observed Stokes parameters from PSR J0437–4715, normalized by the invariant interval and plotted as a function of parallax angle. These data correspond to a pulse phase of approximately 0.485 in Figure 4, as observed in a single 500 kHz channel centered at 1324.75 MHz. The Stokes parameters predicted by the best-fit model are drawn with solid lines.

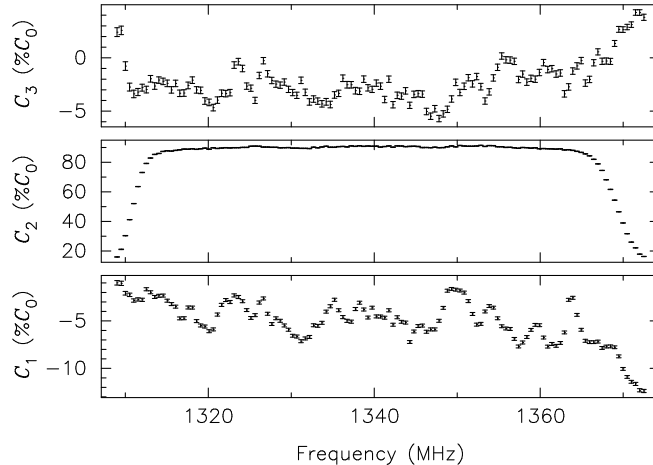


FIG. 2.— Stokes parameters of the noise diode reference signal, plotted as a function of observing frequency. The modeled values of Stokes  $Q$ ,  $U$ , and  $V$  ( $C_1$ ,  $C_2$ , and  $C_3$ ) are specified as percentages of the reference flux density,  $C_0$ . Error bars correspond to the formal standard deviations of the model parameters derived from the best-fit covariance matrix.

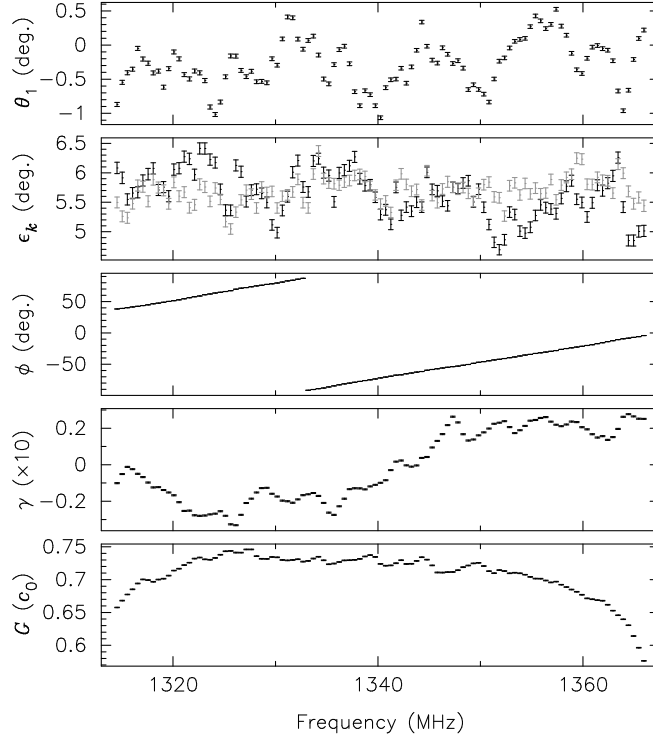


FIG. 3.— Best-fit model parameters as a function of observing frequency. From top to bottom are plotted the orientation of receptor 1 with respect to receptor 0,  $\theta_1$ , the ellipticities of the receptors,  $\epsilon_k$ , the differential phase,  $\phi = \varphi(0)$ , the differential gain,  $\gamma$ , and the absolute gain,  $G$ , specified in units of the square root of the reference flux density,  $c_0 = \sqrt{C_0}$ . In the panel showing the ellipticities, black and grey correspond to receptors 0 and 1, respectively. As in Figure 2, error bars correspond to the formal standard errors of the model parameters.

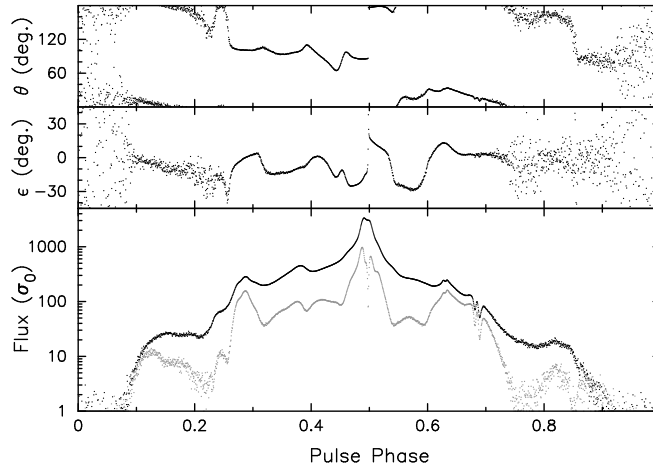


FIG. 4.— Mean polarization of PSR J0437-4715, plotted as a function of pulse phase using polar coordinates: orientation,  $\theta$ , ellipticity,  $\epsilon$ , and polarized intensity,  $S = |\mathbf{S}|$  (plotted in grey below the total intensity,  $S_0$ ). Flux densities are normalized by  $\sigma_0$ , the r.m.s. of the off-pulse total intensity phase bins. Data were integrated over a 64 MHz band centered at 1341 MHz for approximately 8 hours.

## DEGENERACY UNDER COMMUTATION

The Pauli spin matrices satisfy  $\sigma_i \sigma_j = \delta_{ij} \sigma_0 + i\epsilon_{ijk} \sigma_k$ , where  $\epsilon_{ijk}$  is the permutation symbol and summation over the index  $k$  is implied. Using this identity, the product of two arbitrary matrices,  $\mathbf{A}$  and  $\mathbf{B}$ , may be expanded to yield

$$\mathbf{AB} = (a\sigma_0 + \mathbf{a} \cdot \boldsymbol{\sigma})(b\sigma_0 + \mathbf{b} \cdot \boldsymbol{\sigma}) = (ab + \mathbf{a} \cdot \mathbf{b})\sigma_0 + (ab + ba + i\mathbf{a} \times \mathbf{b}) \cdot \boldsymbol{\sigma}. \quad (\text{B1})$$

In this form, it can be seen that  $\mathbf{A}$  and  $\mathbf{B}$  commute if and only if  $\mathbf{a}$  and  $\mathbf{b}$  are collinear, enabling simple statements to be made regarding the uniqueness of solutions to the polarization measurement equation.

For example, consider the parallactic angle rotation given by  $\mathbf{R}_{\hat{\mathbf{v}}}(\Phi) = \cos \Phi \sigma_0 + i \sin \Phi \hat{\mathbf{v}} \cdot \boldsymbol{\sigma}$ . As illustrated by equation (B1), any matrix of the form,  $\mathbf{V} = V_0 \sigma_0 + V \hat{\mathbf{v}} \cdot \boldsymbol{\sigma}$ , commutes freely with  $\mathbf{R}_{\hat{\mathbf{v}}}(\Phi)$ . Therefore, if both  $\mathbf{J}$  and  $\boldsymbol{\rho}_m$  satisfy equation (20), then  $\mathbf{J}^v = \mathbf{J}\mathbf{V}^{-1}$  and  $\boldsymbol{\rho}_m^v = \mathbf{V}\boldsymbol{\rho}_m\mathbf{V}^\dagger$  are also solutions to this equation. This degeneracy exists regardless of the parameterization of  $\mathbf{J}$  or  $\boldsymbol{\rho}_m$ , proving that no unique solution to the polarization measurement equation may be derived solely from observations of unknown sources at multiple parallactic angles.

The consequences of this degeneracy are illustrated by noting that  $\mathbf{V}$  is unimodular and may be decomposed into a boost along the  $\hat{\mathbf{v}}$  axis,  $\mathbf{B}_{\hat{\mathbf{v}}}(\beta_v)$ , and a rotation about this axis,  $\mathbf{R}_{\hat{\mathbf{v}}}(\phi_v)$ . That is, unless  $\mathbf{V}$  is determined through some other means, there remains an unknown position angle error as well as an unknown degree of mixing between the total intensity and circular polarization. An observation of a (possibly unpolarized) source with a well-determined degree of circular polarization may be used to determine  $\beta_v$ ; additionally, an observation of a linearly polarized source with a known position angle (such as the noise diode included in many receiver packages) may be used to constrain  $\phi_v$ .

## REFERENCES

- Britton M. C., 2000, ApJ, 532, 1240  
 Hamaker J. P., Bregman J. D., Sault R. J., 1996, A&AS, 117, 137  
 Hamaker J. P., 2000, A&AS, 143, 515  
 Hanisch R. J., Farris A., Greisen E. W., Pence W. D., Schlesinger B. M., Teuben P. J., Thompson R. W., Warnock A., 2001, A&A, 376, 359  
 Hotan A., van Straten W., Manchester R. N., 2004, A&A, *submitted*  
 Jenet F. A., Anderson S. B., 1998, PASP, 110, 1467  
 Jenet F. A., Cook W. R., Prince T. A., Unwin S. C., 1997, PASP, 109, 707  
 Johnston S., 2002, Proc. Astr. Soc. Aust., 19, 277  
 McKinnon M. M., 1992, A&A, 260, 533  
 Petrova S. A., 2001, A&A, 378, 883  
 Press W. H., Teukolsky S. A., Vetterling W. T., Flannery B. P., 1992, Numerical Recipes: The Art of Scientific Computing, 2<sup>nd</sup> edition. Cambridge University Press, Cambridge  
 Roberts J. A., Cooke D. J., Murray J. D., Cooper B. F. C., Roger R. S., Ribes J.-C., Biraud F., 1975, Aust. J. Phys., 28, 325  
 Stinebring D. R., Cordes J. M., Rankin J. M., Weisberg J. M., Boriakoff V., 1984, ApJS, 55, 247  
 Turlo Z., Forkert T., Sieber W., Wilson W., 1985, A&A, 142, 181  
 van Straten W., 2002, ApJ, 568, 436  
 Xilouris K. M., 1991, A&A, 248, 323